TELKOMNIKA, Vol.15, No.4, December 2017, pp. 1554~1564
ISSN: 1693-6930, accredited **A** by DIKTI, Decree No: 58/DIKTI/Kep/2013
DOI: 10.12928/TELKOMNIKA.v15i4.7234

Image Reconstruction for Solid Profile Measurement in ERT Using Non-invasive Approach

Yasmin Abdul Wahab[1], Ruzairi Abdul Rahim*[2], Mohd Hafiz Fazalul Rahiman[3], Leow Pei Ling[4], Suzanna Ridzuan Aw[5], Muhammad Jayasuman Pusppanathan[6], Mohd Fadzli Abd Shaib[7], Herlina Abdul Rahim[8], Elmy Johana Mohamad[9]
[1]Faculty of Electrical and Electronic Engineering, Universiti Malaysia Pahang,
26600 Pekan, Pahang
[2,4,6,8]Faculty of Electrical Engineering, Universiti Teknologi Malaysia, 81310 Skudai, Johor
[2,7,9]Faculty of Electrical and Electronic Engineering, Universiti Tun Hussein Onn,
86400 Batu Pahat, Johor
[3]School of Mechatronic Engineering, Universiti Malaysia Perlis, 02600 Arau, Perlis
[5]Faculty of Electrical & Automation Engineering Technology, TATiUC,
24000 Kemaman, Terengganu
*Corresponding author, e-mail: yasmin@ump.edu.my[1], ruzairi@fke.utm.my[2], ruzairi@uthm.edu.my[2]

Abstract

Image reconstruction software and its image reconstruction algorithm are an important step towards constructing a tomography system. This paper demonstrates an image reconstruction of solid profile using linear back projection (LBP) algorithm and global threshold. A forward problem and inverse problem are discussed. The modelled of sensitivity distributions using COMSOL proved that the system is able to detect the liquid-solid regime in vertical pipe. Additionally, the location of the phantom can be easily distinguished using LBP algorithm and thresholding technique. The simulations and experiments results indicate that the sensitivity distribution of non-invasive ERT system can be applied in getting a tomogram of the medium of interest.

Keywords*: forward problem, inverse problem, linear back projection algorithm, global threshold*

1. Introduction

Process tomography (PT) has become a promising technique for visualizing and analyzing the internal characteristics of process plants in industry applications, such as for two-phase/multiphase flow in pipelines. This PT has many advantages: low cost, non-invasive, non-intrusive, no radiation hazards, and it is suitable for different size vessels. Therefore, it offers a unique opportunity to reveal the complexity of internal structures of the medium of interest without invading the object.

One of the extensive modalities of PT is Electrical Resistance Tomography (ERT). ERT has been used in many applications such as in geological surface [1–4], agriculture processes [5,6] and also in industrial processes [7]. The advantages of the ERT application are it is relatively safe to use and it provides fast response for online and real-time monitoring of the process plant. There are many examples of ERT systems that have been studied, focusing on imaging technique of the liquid–gas, liquid–liquid or liquid–solid mixtures. However, only a few researchers have considered ERT with a non-invasive sensing technique [8–14]. For non-invasive ERT approach, the electrodes need to be mounted on the periphery of the pipe wall. In addition, its measurement strategy is similar with electrical capacitance tomography (ECT) [13]. This is because a voltage source has been applied to the excitation channel and a current signal is measured at the detection channels.

The ERT is a non-linear model and it is difficult to be solved analytically. Therefore, a finite element model (FEM) is preferable to solve the forward problem in ERT. After that, it has been used with the linearized method to solve the inverse problem.

In this paper, simulations and experiments were used to reconstruct an image of solid profile of non-invasive ERT. The FEM was applied in forward problem to obtain the sensitivity distribution of every pair projections channels. Then, the current-to-voltage measurements for

Received September 2, 2017; Revised November 8, 2017; Accepted November 23, 2017

both homogenous and non-homogenous were recorded. Finally, the concentration profiles of liquid-solid regimes were reconstructed using linear back-projection (LBP) algorithm. A global threshold technique is also applied to the reconstructed image to improve the tomograms. The objective of the current research development and effort is to verify a feasibility and effectiveness of the sensitivity distributions in obtaining the solid profile measurement for the system under investigation.

2. System Overview

The system was modelled using 2D planes in COMSOL Multiphysics, a finite element analysis tool. A 2D dimension model was developed to mimic the real system. The lines representing the width of the sixteen electrodes (E1 – E16) were drawn on the boundary of the pipe surface. The reason for drawing the lines was because the main concern of modelling using COMSOL Multiphysics was the sensor sensitivity.This means that if we give the voltage signal to the electrode, it will allow the electricity to penetrate through the non-conducting pipe, no matter how thick the electrode is. In addition, it is also to avoid a complexity simulation in COMSOL. The 2D geometry of the non-invasive ERT system with sixteen electrodes is shown in Figure 1. The dotted line represents the vertical non-conducting pipe implemented in the real hardware. Also, the outer plane thickness, d was defined to have the same height of the implemented electrode. If the value of d is not defined, by default the COMSOL simulator will set the thickness of the 2D space to be 1 meter.

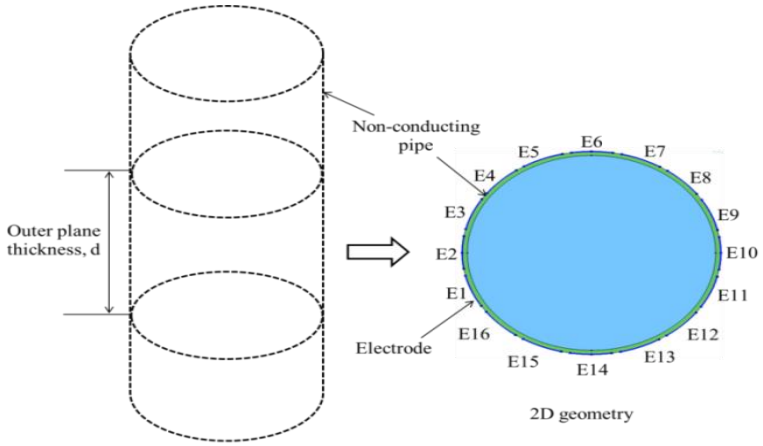

Figure 1. ERT model for non-invasive approach

The material for each related domain in the designed model was defined so that it resembled the real system. The pipe itself was defined as an acrylic medium, whereas the main medium was a tap water. The details of parameters of all materials set in COMSOL Multiphysics are shown in Table 1. A value of electrical conductivity of the tap water was reflected with a measured real tap water used in the real system using a conductor meter, and other materials were based on [15].

Additionally, a complete measurement cycle for a non-invasive ERT system starts with first electrode acts as an excitation electrode and all other electrodes act as detecting electrodes. The excitation electrode is connected to the source and the detecting electrodes are connected to the ground. Thus, the internal resistance is measured between the first electrode and the adjacent electrodes. The process is repeated for all other electrodes until each of the electrodes has become a source electrode, and a complete measurement cycle is done. The electric field and current surface distribution when one electrode was set as the excitation channel and other channels were set as detection electrode is shown in Figure 2.

Table 1. Parameters Defined in COMSOL Multiphysics

Parameter	Value
$\sigma_{acrylic}$; $\varepsilon_{acrylic}$	3.0 ×10^{-14} S/m ; 3.45
σ_{water} ; ε_{water}	7.0 × 10^{-3} S/m ; 80
σ_{wood} ; ε_{wood}	0 S/m ; 2.75
Electrode width (w) x height (h)	16 mm × 200 mm
Number of electrodes	16
Thickness of pipe	2 mm
Inner diameter of pipe	96 mm
Voltage source	10 V, 2 MHz

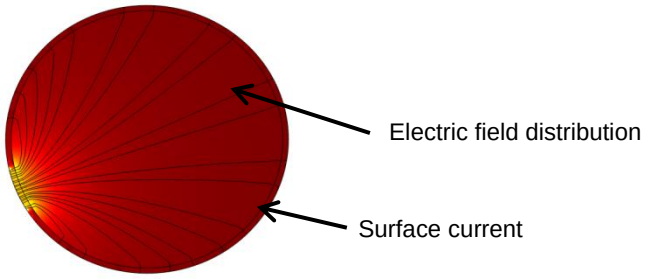

Figure 2. Electric field and surface current distributions for homogenous system

Moreover, a total of sixteen channels of metal electrodes (16 mm (width) × 200 mm (height)) were applied and attached non-invasively to the vertical non-conducting pipe. The non-conducting pipe was an acrylic tube with an outer diameter of 100 mm, a thickness of 2 mm and a height of 500 mm. Each of the metal electrodes was made of a flexible printed circuit board because they could be easily bent. The sensor design is illustrated in Figure 3. The area of the electrode other than the sensing area was shielded by connecting it to the ground to avoid the surrounding noise. Also, a sensor jig was designed to stick and hold each of the sixteen sensors independently. The design of the sensor jig was flexible to ensure that the jig could also be applied to other pipes if necessary. This means that the sensor jig for each the sixteen channels can be unscrewed independently. Simultaneously, a ring holder with two screw locks on the upper and lower sides of the pipe was also designed to hold the sensor jigs.

(a) (b) (c)

Figure 3. Sensor design; (a) outside view of electrode, (b) inner view of electrode, and (c) example electrodes attached at sensor jig and pipe

3. Image Reconstruction

The image reconstruction of process tomography, can be divided into two parts: forward problem and inverse problem [16]. The forward problem is solved first in order to know the theoretical value of each of the sensors output based on the signal projection, whereas the algorithm is solved later in the inverse problem of getting the tomogram.

3.1. Forward Problem

The forward problem also known as the sensitivity map of the system and can be divided into three solutions: linearization solution, numerical solution and analytical solution. The linearization solution is applied when the linear approximation to the relationship of the signal projection of sensors output is made for the system [17]. In addition, the numerical solution – for example, the finite element method (FEM) – is normally used for complex geometry, and the analytical method is used for simple geometry [16]. Most researchers applied numerical solution to solve the forward problem in industrial applications owing to the complex geometry.

For the electrical tomography system such as ERT and ECT, the forward problem is solved by representing the electrical field distribution of the internal system [18]. Moreover, the ERT, ECT and non-invasive ERT electrodes are governed by Poisson's equations with only different coefficient values and boundary conditions. Thus, it should be solved depending on the types of electrical tomography system as described by Sun and Yang [19] for ERT and Lei *et al.* [20] for ECT. As a result, based on references by Lionheart [18] and Sun and Yang [21], the sensitivity coefficient of a two-dimensional electrode pair for non-invasive ERT is based on Equation (1).

$$M_{i,j}(x,y) = \frac{\Delta G}{\Delta \sigma} = \int_{A(x,y)} \frac{\boldsymbol{E}_i}{V_i} \cdot \frac{\boldsymbol{E}_j}{V_j} dxdy \tag{1}$$

According to Equation (1), the sensitivity coefficient for pair electrode *i-j*, $M_{i,j}(x,y)$ to the conductivity change of the pixel at position (x,y) within the area $A(x,y)$ is solved by using dot-multiplying between the *i*-electric field, $\boldsymbol{E}_i$, and *j*-electric field, $\boldsymbol{E}_j$, when voltage source V_i and V_j are applied, respectively. COMSOL Multyphysics live linked with MATLAB has been utilized in this work to solve the forward problem for the non-invasive ERT system. For every excitation channels, the electric field projection inside the pipe was exported according to how many pixels are involved. For this research, 128 × 128 pixels are the pixels concerned. Later, the sensitivity coefficient for each electrode pair is obtained by the dot product of two electric fields.

The sensitivity map for each pair projection between channel 1 and other channels modelled by using COMSOL is illustrated in Figure 4. It can be seen that the projection for each pair of electrodes produces a curved line. The curved line occurred owing to the soft-field behavior of the electrical tomography. The soft-field nature produces a poor condition for sensitivity distribution in electrical tomography, which becomes gradually poorer when it moves towards the center of the vessel region [22]. In other words, the sensitivity distribution for electrical tomography is more sensitive near to the electrodes. Also, the projection value of adjacent electrodes pairs (E1E2 and E1E16) are larger compared to the opposite electrode pair, which indicates that it failed to give a uniform and even sensitivity distribution. This is because of distinctive soft-field sensing characteristics [23].

3.2. Inverse Problem

After the sensitivity map of the system has been solved, the tomogram is obtained. There are numerous method of reconstructing image in ERT, either using a non-iterative or an iterative algorithm [24]. However, the non-iterative method is chosen in this work because it is simple and quick [25]. A back-projection algorithm is categorized as a non-iterative algorithm [26]. It is a famous technique in tomography application such as a linear back-projection (LBP) algorithm, and filtered-back projection algorithm. But, only the LBP algorithm was a concern in this work.

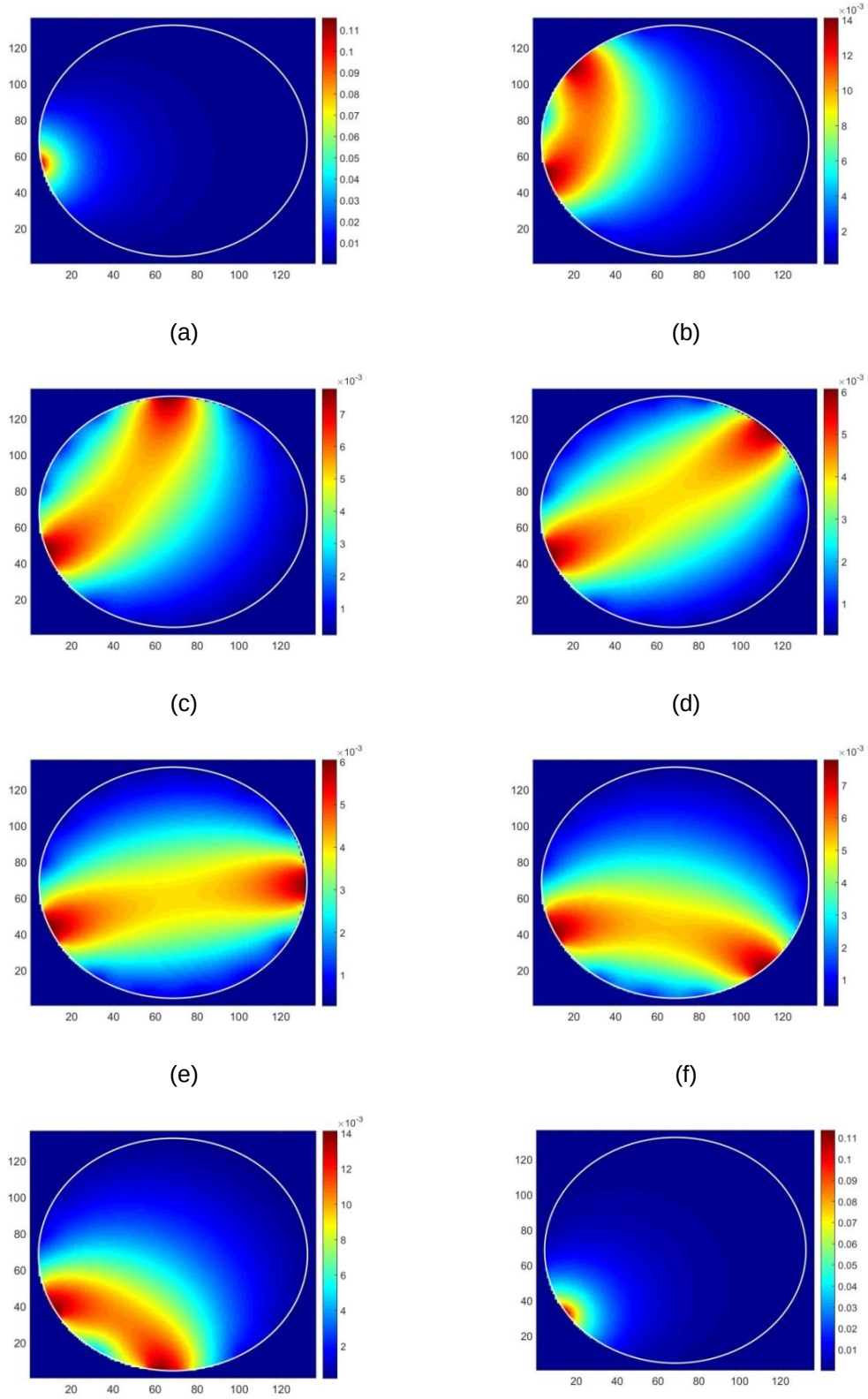

Figure 4. Sensitivity map for ; (a) electrode 1 and 2, (b) electrode 1 and 4, (c) electrode 1 and 6, (d) electrode 1 and 8, (e) electrode 1 and 10, (f) electrode 1 and 12, (g) electrode 1 and 14, and (h) electrode 1 and 16

3.2.1. Linear Back Projection Algorithm

LBP is applied in many tomography processes, such as in ultrasonic tomography [27–30], optical tomography [31–34], electrical resistance tomography [14,19], [35,36] and electrical capacitance tomography [37–41]. The advantages of the LBP algorithm is its low computational complexity, and it can generate an image at high speed [25]. In reconstructing the image using LBP, each sensitivity matrix is multiplied with its corresponding sensor reading [42]. The back-projected data values are smeared back across the unknown density function (image) and overlap each other to increase the projection data density [28]. Hence, the main disadvantage of LBP algorithm is that it produces a blurred image, also known as the smearing effect [43]. Knowing that, the tomogram obtained by the LBP algorithm is not so clear, but is still sufficient to identify the medium of interest.

The LBP involves the matrix multiplication between the normalizing sensitivity map, $\overline{M}_{i,j}(x,y)$ and the signal loss amplitude of receiver *j*-th for projection *i*-th, $S_{i,j}$ [42, 44]. Then the same element of the arrays will be summed to get the back-projected conductivity distribution, also known as the concentration profile. Consequently, the concentration profile will be displayed in colour pixels. The mathematical equation of LBP can be expressed as follows:

$$P_{LBP}(x,y)=\sum_{i=1}^{16}\sum_{j=1}^{16}\overline{M}_{i,j}(x,y)\times S_{i,j} \tag{2}$$

In this study, the tomogram obtained by the LBP algorithm was standardized from 0 to 1 by using Equation (3) for easy comparison and analysis.

$$P_{LBPnorm}(x,y)=\frac{P_{LBP(m,n)}(x,y)-P_{LBP\min}(x,y)}{P_{LBP\max}(x,y)-P_{LBP\min}(x,y)} \tag{3}$$

where

$P_{LBP}(x,y)$ is the conductivity distribution obtained using LBP algorithm or the concentration profile,

m and n are the specified location of 136 × 136 pixels of the concentration profile,

$P_{LBPnorm}(x,y)$ is the normalized concentration profile,

$P_{LBP(m,n)}(x,y)$ is the pixel value at m and n of the concentration profile,

$P_{LBP\min}(x,y)$ is the minimum value of pixel in the concentration profile, and

$P_{LBP\max}(x,y)$ is the maximum value of pixel in the concentration profile.

3.2.2. Thresholding Technique

The thresholding technique can be used to extract objects from the background [45]. In the tomography application, it can improve the quality of the reconstructed image by removing the unwanted pixels in the cross-section image, and the minor medium, such as gas or solid concentration, can be identified. The basic thresholding technique involves the intensity of pixels in the concentration profile that are converted into a binary value depending on the threshold value, P_{Th} [46]. This is also known as the global threshold [45]. If the pixel value is greater than the pre-set threshold, the final pixel is set to 1 or is otherwise 0. Equation (4) shows the mathematical model of the thresholding process for a given reconstructed image from the LBP algorithm. $G_T(x,y)$ is the resulting image after the thresholding process that has been applied in this work. However, the threshold value must be carefully selected to ensure that the improved reconstructed image is reasonable. For that reason, the method to choose the best threshold value was done by taking 100 steps (with interval 0.01) of the pixel value of the concentration profile. Accordingly, the area error (AE) was determined, and the optimum threshold value that gave AE value to be almost +/- 0 was selected. Then the mean of the optimum threshold value for all types of simulations or experiments conducted was calculated

and implemented for the final thresholding process. For this paper, the average ratio of threshold value applied for image reconstruction was 0.91 (experiment) and 0.92 (simulation).

$$G_T(x,y)=\begin{cases}1, if\ P_{LBPnorm(m,n)}(x,y) > P_{Th}\\ 0, if\ P_{LBPnorm(m,n)}(x,y) \le P_{Th}\end{cases} \quad (4)$$

4. Results and Discussions

Figure 5 shows the solid concentration profile at a different sizes and positions with comparison between LBP and threshold approach. A solid rod each with diameter 12 mm and 20 mm was used as a single phantom. Also, double phantoms of 12 mm in diameter were tested. The results from simulations were done by obtaining the sensors reading from COMSOL, while an online configuration was applied to get the sensors reading from the experiments. Moreover, the experiments were done to validate the results from the simulations. It can be observed that the LBP algorithm was able to identify and distinguish the sizes and positions of the solid profile. That aside, the circular shapes of the phantoms were not exactly identical to the reference image. The smearing effect from the LBP and the placement of the phantom near to the pipe wall caused the non-identical shape of the tomogram.

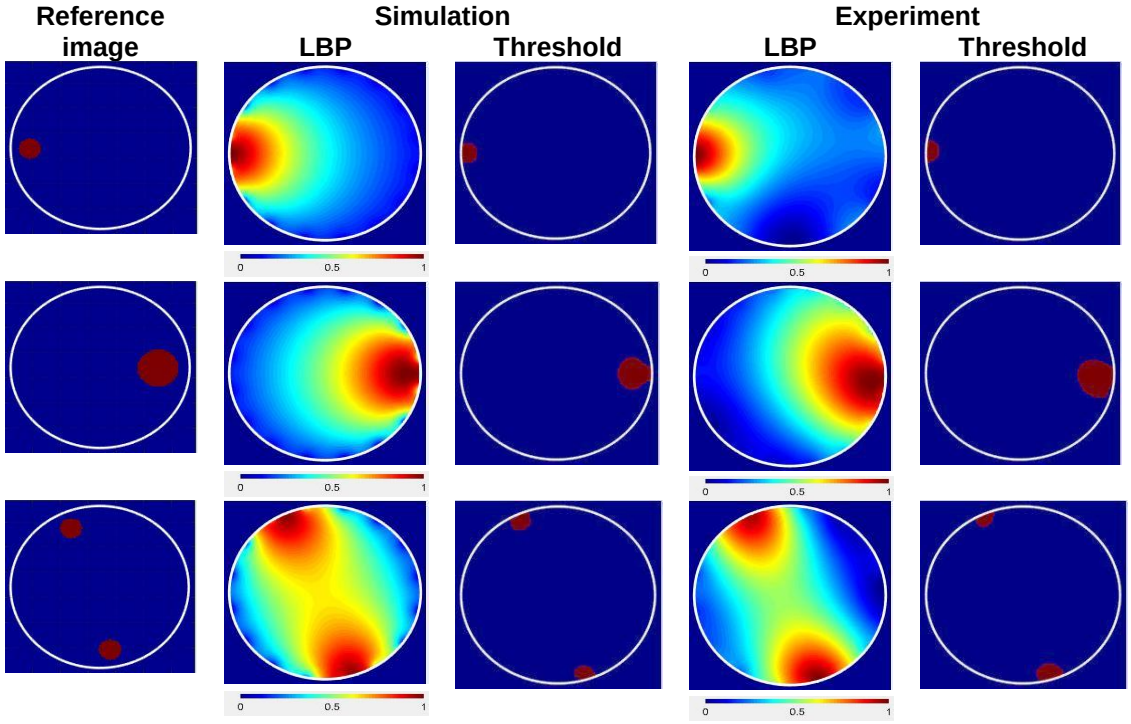

Figure 5. Reconstructed images between simulation and experiment

Besides, the results of the tomograms from thresholding approach are presented in pseudo-colour, which is red and blue, for binary value 1 and 0, respectively. The threshold approach was used to improve the resulted images obtained from the LBP algorithm. It can be seen that the smearing effect surrounding the phantoms were eliminated using the threshold technique. However, it was believed that the main failure of getting a good reconstructed image as clear as the reference image is because the image reconstruction was basically reconstructed from the LBP algorithm. The blurred image obtained from LBP and applied for the threshold technique influenced the reconstructed image. It affected a pre-set threshold value of threshold technique for each experiments, as well as the average ratio made of the pre-

set threshold, and so produced non-ideal images. But, it still gave sufficient information so that the system could detect phantoms in the vertical column.

The performance of the tomograms is examined further by using multi scale structural similarity (MSSIM). The MSSIM is a technique that compares the similarity between the resulted image and the reference image [47,48]. The MSSIM results in the output between the indexes 0 to 1. A larger value of the MSSIM index will indicates that the reconstructed image closer to the reference image. A detailed explanation on MSSIM can be found in Ref. [47–49]. Figure 6 illustrates the MSSIM index for tomograms obtained from Figure 5. Generally, the graphs pattern for simulation and experiment from LBP and threshold were similar for each other. Besides, the threshold approach gave a large value of MSSIM index compared to the LBP approach. The value of MSSIM index using threshold method for all phantoms tested were larger than 0.9. However, the LBP technique only results the MSSIM index below than 0.2 for both simulation and experiment. Thus, it is observed that the threshold approach gave a better results of image reconstruction because it near to the index one and resulting similar to the reference image.

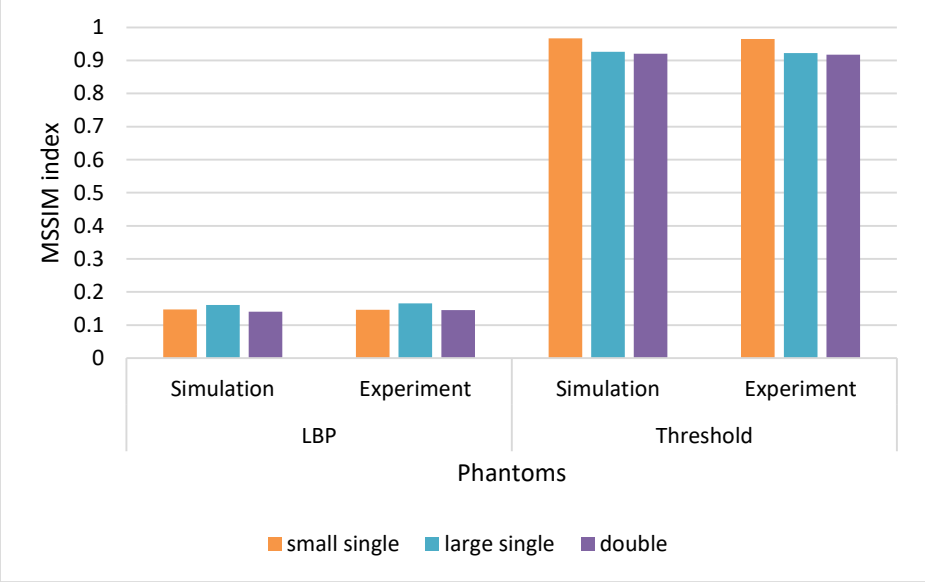

Figure 6. MSSIM index versus different phantoms

5. Conclusion

A sensitivity distribution and implementation of LBP algorithm of ERT using non-invasive approach indicates that the system was able to detect the concentration profile of liquid-solid two-phase regime. It also proved that a correct sensitivity map is very important as it is a crucial in solving an inverse problem part towards producing a correct image reconstruction. The smearing effect was eliminated when using global threshold technique. However, as LBP used as a basic algorithm, thus the exactly shape of the reference image cannot be obtained. Moreover, the image quality assessment using MSSIM also indicates that the threshold approach produces a better results of image reconstruction compared to the LBP algorithm because the values were near to index 1. Future work will focus on implementing other algorithm such as iterative algorithm for better tomogram.

Acknowledgement

The authors would like to thank the Ministry of Higher Education and University Malaysia Pahang for funding the study. Very special thanks go to Universiti Teknologi Malaysia, PROTOM research group for their generous support and cooperation, and UTM grant (M53) for funding this project.

References

[1] E Auken, J Doetsch, G Fiandaca, AV Christiansen, A Gazoty, AG Cahill, R Jakobsen. Imaging Subsurface Migration of Dissolved CO2 in A Shallow Aquifer using 3-D Time-Lapse Electrical Resistivity Tomography. *Journal of Applied Geophysics*. 2014; 101: 31–41.

[2] SD Carrière, K Chalikakis, G Sénéchal, C Danquigny, C Emblanch. Combining Electrical Resistivity Tomography and Ground Penetrating Radar to study geological structuring of karst Unsaturated Zone. *Journal of Applied Geophysics*. 2013; 94: 31–41.

[3] J Qiyun, H Jishan, S Ping, P Jing. *The Hardware Design of a Mine Resistivity Tomography Instrument*. Proceedings of the 2009 IEEE International Workshop on Imaging Systems and Technique. Shenzhen, China. 2009: 235–238.

[4] RL Newmark, AL Ramirez, WD Daily. Monitoring Carbon Dioxide Sequestration using Electrical Resistance Tomography (ERT): A Minimally Invasive Method. *Greenhouse Gas Control Technologies*. 2003; I: 353–358.

[5] S Garré, I Coteur, C Wongleecharoen, K Hussain, W Omsunrarn, T Kongkaew, T Hilger, J Diels, J Vanderborght. *Can We Use Electrical Resistivity Tomography to Measure Root Zone Dynamics in Fields with Multiple Crops?* Procedia Environmental Sciences. Kyoto, Japan. 2013; 19: 403–410.

[6] J Boaga, M Rossi, G Cassiani. *Monitoring Soil-plant Interactions in an Apple Orchard Using 3D Electrical Resistivity Tomography*. Procedia Environmental Sciences. Kyoto, Japan. 2013; 19: 394–402.

[7] M Sharifi, B Young. Electrical Resistance Tomography (ERT) Applications to Chemical Engineering. *Chemical Engineering Research and Design*. 2013; 91: 1625–1645.

[8] Z Cao, L Xu, C Xu, H Wang. *Electrical Resistance Tomography (ERT) by using An ECT Sensor*. Proceedings of the 2010 IEEE International Conference on Imaging Systems and Techniques. Thessaloniki, Greece. 2010: 63–66.

[9] BL Wang, ZY Huang, HF Ji, HQ Li. *Towards Capacitively Coupled Electrical Resistance Tomography*. Proceedings of the 6th World Congress on Industrial Process Tomography. Beijing, China. 2010: 1574–1577.

[10] B Wang, Y Hu, H Ji, Z Huang, H Li. *A Novel Electrical Resistance Tomography System Based on C4D Technique*. Proceedings of the 2012 IEEE International Conference on Instrumentation and Measurement Technology. Graz, Austria. 2012: 1929–1932.

[11] Y Li, M Soleimani. Imaging Conductive Materials with High Frequency Electrical Capacitance Tomography. *Measurement*. 2013; 46(9): 3355–3361.

[12] B Wang, Y Hu, H Ji, Z Huang, H Li. A Novel Electrical Resistance Tomography System Based on C4D Technique Technique. *IEEE Transactions on Instrumentation and Measurement*. 2013; 62(5): 1017–1024.

[13] B Wang, W Zhang, Z Huang, H Ji, H Li. Modeling and Optimal Design of Sensor for Capacitively Coupled Electrical Resistance Tomography System. *Flow Measurement and Instrumentation*. 2013; 31: 3–9.

[14] B Wang, W Tan, Z Huang, H Ji, H Li. Image Reconstruction Algorithm for Capacitively Coupled Electrical Resistance Tomography. *Flow Measurement and Instrumentation*. 2014; 40: 216–222.

[15] J William, H Hayt, JA Buck. Engineering Electromagnetics, Seven Edition. New York: Mc Graw Hill. 2006: 552–553.

[16] G Dong, J Zou, RH Bayford, X Ma, S Gao, W Yan, M Ge, AG Equation. The Comparison Between FVM and FEM for EIT Forward Problem. *IEEE Transactions on Magnetics*. 2005; 41(5): 1468–1471.

[17] GR Shaw, Y Goussard, R Guardo. *Linearization of the Forward Problem in Electrical Impedance Tomography*. Proceedings of the IEEE International Conference on Engineering in Medicine and Biology Society. California, USA. 1993; 2: 82–83.

[18] WRB Lionheart. *Reconstruction Algorithms for Permittivity and Conductivity Imaging*. Proceedings of the 2001 World Congress on Industrial Process Tomography. Hannover, Germany; 2001: 4–11.

[19] J Sun, W Yang. Evaluation of Fringe Effect of Electrical Resistance Tomography Sensor. *Measurement*. 2014; 53: 145–160.

[20] J Lei, S Liu, X Wang, Q Liu. An Image Reconstruction Algorithm for Electrical Capacitance Tomography Based on Robust Principle Component Analysis. *Sensors*. 2013; 13(2): 2076–92.

[21] J Sun, W Yang. A Dual-Modality Electrical Tomography Sensor for Measurement of Gas–Oil–Water Stratified Flows. *Measurement*. 2015; 66: 150–160.
[22] S Mohammad. Segmented Excitation for Electrical Capacitance Tomography. Master Thesis. Skudai: Universiti Teknologi Malaysia. 2012.
[23] EJ Mohamad. A Segmented Capacitance Tomography for Visualising Material Distributions in Pipeline Conveying Crude Plam Oil. PhD Thesis. Skudai: Universiti Teknologi Malaysia. 2012.
[24] Wael AD. Electrical Capacitance Tomography for Conductive Materials. PhD Thesis. Cookeville: Tennessee Technological University. 2010.
[25] J Lei, S Liu. Dynamic Inversion Approach for Electrical Capacitance Tomography. *IEEE Transactions on Instrumentation and Measurement*. 2013; 62(11): 3035–3049.
[26] Z Zakaria. Non-Invasive Imaging of Liquid/Gas Flow using Ultrasonic Transmission Mode Tomography. Master Thesis. Skudai: Universiti Teknologi Malaysia. 2007.
[27] NMN Ayob, S Yaacob, Z Zakaria, MHF Rahiman, RA Rahim, MR Manan. *Improving Gas Component Detection of an Ultrasonic Tomography System for Monitoring Liquid / Gas Flow*. Proceedings of the 2010 6th IEEE International Colloquium on Signal Processing & Its Applications. Malacca, Malaysia. 2010: 278–282.
[28] Z Zakaria, MHF Rahiman, RA Rahim. Simulation of the Two-Phase Liquid–Gas Flow through Ultrasonic Transceivers Application in Ultrasonic Tomography. *Sensors & Transducer*. 2010; 112(1): 24–38.
[29] MHF Rahiman, RA Rahim, J Pusppanathan. Two-Phase Flow Regime Identification by Ultrasonic. *Sensors & Transducer*. 2010; 116(5): 76–82.
[30] MHF Rahiman, RA Rahim, HA Rahim, NMN Ayob. The Hardware Design Technique for Ultrasonic Process. *Sensors & Transducer*. 2012; 141(6): 52–61.
[31] SZM Muji, RA Rahim, MHF Rahiman, Z Tukiran, NMN Ayob, EJ Mohamad, MJ Puspanathan. Optical Tomography: Image Improvement Using Mixed Projection of Parallel and Fan Beam Modes. *Measurement*. 2013; 46(6): 1970–1978.
[32] M Wei, M Tong, J Hao, L Cai, J Xu. Detection of Coal Dust in A Mine Using Optical Tomography. *International Journal of Mining Science and Technology*. 2012; 22(4): 523–527.
[33] S Ibrahim, MAM Yunus, RG Green, K Dutton. Concentration Measurements of Bubbles in A Water Column using An Optical Tomography System. *ISA Transactions*. 2012; 51(6): 821–826.
[34] J Jamaludin, RA Rahim, HA Rahim, MHF Rahiman, SZM Muji, JM Rohani. Charge Coupled Device Based on Optical Tomography System in Detecting Air Bubbles in Crystal Clear Water. *Flow Measurement and Instrumentation*. 2016; 50: 13–25.
[35] T Dyakowski, LFC Jeanmeure, AJ Jaworski. Applications of Electrical Tomography for Gas–Solids and Liquid–Solids Flows — A review. *Powder Technology*. 2000; 112(3): 174–192.
[36] P Wang, B Guo, N Li. Multi-Index Optimization Design for Electrical Resistance Tomography Sensor. *Measurement*. 2013; 46(8): 2845–2853.
[37] Z Cui, H Wang, C Yang, D Zhang, Y Geng. *Development and Application of ECT Digital System for Online Flow Measurement*. Proceedings of the 2012 IEEE International Conference on Imaging Systems and Techniques. Manchester, United Kingdom. 2012: 599–604.
[38] EJ Mohamad, RA Rahim. *Multiphase Flow Reconstruction in Oil Pipelines by Portable Capacitance Tomography*. Proceedings of the 2010 IEEE Sensors. Hawaii. 2010: 273–278.
[39] WQ Yang, L Peng. Image Reconstruction Algorithms for Electrical Capacitance Tomography. *Measurement Science and Technology*. 2003; 14: R1–R13.
[40] Y Chen, L Zhang, D Chen. *Two-Phase Flow Parameters Measurement and Image Reconstruction for Electrical Capacitance Tomography*. Proceedings of the 2008 IEEE International Workshop on Education Technology and Training & International Workshop on Geoscience and Remote Sensing. Shanghai, China. 2008: 680–684.
[41] MJ Pusppanathan, FR Yunus, NMN Ayob, RA Rahim, FA Phang. A Novel Electrical Capacitance Sensor Design for Dual Modality. *Jurnal Teknologi*. 2013; 5: 45–47.
[42] SYNMN Ayob, MHF Rahiman, Z Zakaria, RA Rahim. Eminent Pixel Reconstruction Algorithm for Ultrsonic Tomography. *Jurnal Teknologi*. 2011; 55(2): 15–22.

[43] W Warsito, L Fan. Measurement of Real-Time Flow Structures in Gas–Liquid and Gas-Liquid–Solid on Systems using Electrical Capacitance Tomography (ECT). *Chemical Engineering Science*. 2001; 56: 6455–6462.
[44] MHF Rahiman, RA Rahim. A Novel Hybrid Binary Reconstruction Algorithm for Ultrasonic Tomography. *Sensors & Transducer*. 2008; 89(3): 93–100.
[45] RC Gonzalez, RE Woods. Digital Image Processing. Second Edition. New Jersey: Prentice Hall. 2010.
[46] ILS Mei, IB Ismail, A Bawadi, A Shafquet. Evaluation of Electrical Capacitance Tomography Thresholding Techniques for Void Fraction Measurement of Gas-Liquid System. *Applied Mechanics and Materials*. 2014; 625: 439–443.
[47] Z Wang, AC Bovik, HR Sheikh, EP Simmoncelli. Image Quality Assessment: From Error Visibility to Structural Similarity. *IEEE Transactions on Image Processing*. 2004; 13(4): 600–612.
[48] Z Wang, AC Bovik, L Lu. *Why is Image Quality Assessment So Difficult?* Proceedings of the 2002 IEEE International Conference on Acoustics Speech and Signal Processing. Florida, USA. 2002; 303: 3313–3316.
[49] Z Wang, AC Bovik. Error : Love It or Leave It ? *IEEE Signal Processing Magazine*. 2009; 6(January): 98–117.